RSC Advances

PAPER

Cite this: *RSC Adv.*, 2020, **10**, 7585

Biferrocenyl Schiff bases as efficient corrosion inhibitors for an aluminium alloy in HCl solution: a combined experimental and theoretical study†

Uzma Nazir,[a] Zareen Akhter,*[a] Naveed Kausar Janjua,[a] Muhammad Adeel Asghar,[a] Sehrish Kanwal,[a] Tehmeena Maryum Butt,[a] Asma Sani,[a] Faroha Liaqat,[a] Rizwan Hussain[b] and Faiz Ullah Shah*[c]

The corrosion inhibitive capabilities of some ferrocene-based Schiff bases on aluminium alloy AA2219-T6 in acidic medium were investigated using Tafel polarization, electrochemical impedance spectroscopy (EIS), weight loss measurement, FT-IR spectroscopy and scanning electron microscopic (SEM) techniques. The influence of molecular configuration on the corrosion inhibition behavior has been explored by quantum chemical calculation. Ferrocenyl Schiff bases 4,4′-((((ethane-1,2-diylbis(oxy))bis(4,1-phenylene))bis(methaneylylidene)) bis(azaneylylidene))bisferrocene (**Fcua**), 4,4′-((((ethane-1,2-diylbis(oxy))bis(2-methoxy-1,4-phenylene)) bis(methaneylylidene))bis(azaneylylidene))bisferrocene (**Fcub**) and 4,4′-((((ethane-1,2-diylbis(oxy))bis(2-ethoxy-1,4-phenylene))bis(methaneylylidene))bis(azaneylylidene))bisferrocene (**Fcuc**) have been synthesized and characterized by FT-IR, ^{1}H and ^{13}C NMR spectroscopic studies. These compounds showed a substantial corrosion inhibition against aluminium alloy in 0.1 M of HCl at 298 K. **Fcub** and **Fcuc** showed better anticorrosion efficiency as compared with **Fcua** due to the electron donating methoxy and ethoxy group substitutions, respectively. Polarization curves also indicated that the studied biferrocenyl Schiff bases were mixed type anticorrosive materials. The inhibition of the aluminium alloy surface by biferrocenyl Schiff bases was evidenced through scanning electron microscopy (SEM) studies. Semi-empirical quantum mechanical studies revealed a correlation between corrosion inhibition efficiency and structural functionalities.

Received 18th December 2019
Accepted 10th February 2020

DOI: 10.1039/c9ra10692h

rsc.li/rsc-advances

1 Introduction

Schiff bases, compounds having an azomethine (>C=N–) linkage, are an essential class of organic compounds used in coordination chemistry as chelating ligands.[1] The presence of nitrogen and oxygen donor atoms in such compounds make them structurally similar to the neutral biological systems and are utilized in elucidating the mechanism of transformation of racemization reactions.[2,3] During the last three decades, interest in ferrocene-based compounds has immensely increased owing to their favorable electronic properties, ease of functionalization and exceptional stability towards water and air.[4] Numerous chemical properties have made ferrocene a striking molecule in a variety of applications. They have promising electrochemical properties and are usually non-toxic.[5] These properties make them suitable candidates for various applications in materials science including the design of new catalytic materials and organic synthesis, redox sensors for molecular recognition, electroactive and aerospace materials.[6,7] Schiff bases having a ferrocene moiety have drawn substantial consideration due to their superior anticancer and free-radical scavenging properties.[8] Other industrial applications of ferrocene derivatives include their use as additives for heating oil to diminish smut formation, protective coatings for satellites and rockets, and UV absorbers.[9]

Corrosion of materials is considered as one of the worst technical problems faced by nearly all industries. It is a crucial process that is adversely affecting the properties of materials in contact with surroundings. Hydrochloric acid is one of the most important agents being used as an acid catalyst and as a heat exchanger in industries, for removing undesired scale, rust and cleaning of boilers. Regardless of the extraordinary developments in corrosion science and technology, the phenomenon of corrosion remains a foremost obstacle for industries all over the world. Though corrosion can be controlled by adopting suitable methods and highly corrosion resistant materials, it accounts for additional expenditures and economic losses. Schiff bases has already shown corrosion inhibition properties for metals and alloys in acidic media.[10] The popularity of Schiff bases has increased due to their cost effective starting materials, facile

[a]*Department of Chemistry, Quaid-i-Azam University, Islamabad-45320, Pakistan. E-mail: zareen_a@qau.edu.pk*

[b]*Laboratory for Advanced Materials Processing (LAMP), NCP, Islamabad, Pakistan*

[c]*Chemistry of Interfaces, Luleå University of Technology, 971 87 Luleå, Sweden. E-mail: faiz.ullah@ltu.se*

† Electronic supplementary information (ESI) available. See DOI: 10.1039/c9ra10692h

route of synthesis, low toxicity,[11] high purity and environment friendly nature.[12–15] Corrosion studies of aluminium metal and its alloys have received significant consideration because of their extensive industrial applications and economic impacts.[16] Aluminium metal and its alloys have emerged as alternate materials in some chemical processing and in aerospace industries. Due to their widespread applications, they regularly interact with acids or bases for the period of curing, de-scaling and electrochemical etching.

There are of two types of mode of adsorption of the anti-corrosive molecules: chemical adsorption process in which coordinate type bond is formed by transfer of charge or sharing of charge from the organic molecules to low-energy vacant orbital of the metal surface while physical adsorption involves electrostatic interaction between electrically charged metal surface and the charged inhibitor molecules.[17,18]

In acidic medium, the anticorrosion efficiency of aluminium alloy has a pronounced significance. For the protection of metal against acid corrosion, the most common approaches include the use of inorganic and organic compounds having functional groups containing non-bonding electrons on the heteroatoms, such as oxygen (–O–, $-OCH_3$, $-OC_2H_5$); nitrogen atoms (>C=N), π electrons in aromatic ring and ferrocene moiety in their structure. Schiff base compounds are considered as proficient anticorrosive materials due to the presences of –C=N group.[19]

The anticorrosive efficiency of organic Schiff base compounds are reported on steel, copper,[19–25] pure aluminium and its alloys,[16,23,26] and ferrocene derivatives for mild steel in the acidic medium.[4,7,27,28] According to the existing literature, not much research has been carried out regarding the inhibition of corrosion on aluminium alloys of the series 2000 *i.e.* aluminium alloy AA2219-T6 in acidic medium. Therefore, there is an urgent need for the development of novel corrosion inhibitors for aluminium alloys of the series 2000. Thus, it was thought worthy to design and synthesize new biferrocenyl Schiff bases and investigate their corrosion inhibitive behaviour on AA2219-T6 alloy in mild acidic medium.

We have recently investigated the corrosion inhibitive behavior on this particular alloy through the organicanalogues of these Schiff bases and have revealed promising performance.[29] The present work is aimed at investigating the corrosion inhibitive performance of three newly synthesized biferrocenyl Schiff bases such as 4,4′-(((((ethane-1,2-diylbis(oxy))bis(4,1-phenylene)) bis(methaneylylidene))bis(azaneylylidene))bisferrocene (**Fcua**), 4,4′-((((ethane-1,2-diylbis(oxy))bis(2-methoxy-1,4-phenylene)) bis(methaneylylidene))bis(azaneylylidene))bisferrocene (**Fcub**) and 4,4′-((((ethane-1,2-diylbis(oxy))bis(2-ethoxy-1,4-phenylene)) bis (methaneylylidene))bis(azaneylylidene))bisferrocene (**Fcuc**). Aluminium alloy surface morphology was investigated by FT-IR spectroscopy and scanning electron microscopic (SEM) technique. The presence of –CH=N– group, the electronegative oxygen and nitrogen atoms, an electron cloud on the aromatic ring and presence of ferrocene moiety in the investigated Schiff base molecules render them as promising anticorrosive materials for aluminium alloy.[30] The gravimetric analysis, polarization and electrochemical impedance methods were used to evaluate the anticorrosive effect of these biferrocenyl Schiff base compounds. Moreover, quantum chemical calculations have been performed employing semi-empirical method (using basis set PM6) to investigate the anticorrosion mechanism and its correlation with electronic and structural properties of the organometallic inhibitors. The corresponding relationship between inhibition effectiveness and theoretical parameters, such as the highest occupied molecular orbital (E_{HOMO}) and the lowest unoccupied molecular orbital (E_{LUMO}), the energy band gap ΔE, electronegativity (χ), dipole moment (μ) and other structural parameters of the concerned compounds has been investigated in detail.

2 Experimental

2.1 Materials and methods

All chemicals attained from commercial sources were of analytical grade and used for experiments as received. 4-Hydroxybenzaldehyde, 4-hydroxy-3-methoxybenzaldehyde, hexadecyltrimethylammonium bromide, 3-ethoxy-4-hydroxybenzaldehyde were obtained from Fluka in pure form. Ferrocene, sodium nitrite, palladium charcoal, nitroaniline, hydrazine, hydrochloric acid and anhydrous potassium carbonate were obtained in pure form. Dichloroethane was purchased from Merck. Absolute ethanol, dimethyl formamide (DMF), dichloromethane and diethyl ether were further purified before use, following the standard method.[31]

Bruker AXR, 300 MHz spectrometer was used for recording ^{1}H NMR and ^{13}C NMR spectra. Vibration frequencies of all biferrocene Schiff bases were recorded through FT-IR spectra on ATR with PerkinElmer System 2000. Electrochemical studies were done with the help of a Potentiostat/Galvanostat (Gamry interface 1000).

2.2 Preparation of Schiff bases

Synthesis of ferrocenyl aniline was carried out in two steps using the previously reported method,[32] with slight modifications to get a better yield of about 61–67%. The diformyl precursors were prepared by refluxing hydroxyl benzaldehyde with appropriate 1,2-dichloroethane using DMF as a solvent. Schiff bases having ferrocene moiety were synthesized by condensation of the corresponding diformyl compound with ferrocenyl aniline. The general method used for the preparation of ferrocenyl Schiff bases is briefly described here. In a round bottom flask of 250 mL furnished with a magnetic stirrer and a condenser, 1 mol of corresponding dialdehyde was dissolved in dried 50 mL absolute ethanol and then 2.1 mol of ferrocenylaniline dissolved in 30 mL absolute ethanol was added dropwise to this solution within 30 minutes under inert atmosphere. The mixture was heated at 90 °C to reflux for 6–7 hours; the formation of product was observed by TLC [*n*-hexane/ethyl acetate (6 : 4)]. After the completion of reaction, the mixture was cooled and golden colored ferrocene Schiff base thus attained was filtered and recrystallized with dried ethanol to get the corresponding Schiff base. The general reaction is also shown in Scheme 1.

2.2.1 Synthesis of 4,4′-((((ethane-1,2-diylbis(oxy))bis(4,1-phenylene))bis(methaneylylidene))bis(azaneylylidene))bisferrocene (Fcua). The Schiff base **Fcua** was synthesized by the above-mentioned procedure using dialdehyde (0.2 g, 0.740 mmol) 4,4′-diformyldiphenoxy ethane with (0.456 g, 1.64 mmol) 4-ferrocenyl aniline. Yield 65%; mp 180 °C; FT-IR (ν cm^{-1}): ν(C=N) 1602; ν(C–O–C) 1240; (Fe–cp) 486. ^{1}H NMR ($CDCl_3$; δ ppm): 8.49 (1H, HC=N); 4.68 (s, 2H, J = 1.8 Hz, C_5H_4), 4.67 (s, 2H, J = 1.8, C_5H_4). 4.07 (s, 5H, C_5H_5); ^{13}C NMR ($CDCl_3$; δ ppm) 159.14 (HC=N); 85.06 (1C), 68.97 (4C) (Cp–C sub); 66.38 (Cp–C unsub); 69.63 (aliphatic C, –C_2H_4–).

2.2.2 Synthesis of 4,4′-((((ethane-1,2-diylbis(oxy))bis(2-methoxy-1,4-phenylene))bis(methaneylylidene))bis(azaneylylidene))bisferrocene (Fcub). The Schiff base **Fcub** was synthesized by aforementioned procedure using (0.2 g, 0.606 mmol) 4,4′-diformyl-bis-methoxydiphenoxy ethane with (0.353 g, 1.26 mmol) 4-ferrocenyl aniline. Yield 61%; mp 210 °C; IR (ν cm^{-1}): ν(C=N) 1580; ν(C–O–C) 1235; ν (Fe–cp) 486. ^{1}H NMR ($CDCl_3$; δ ppm): 8.37 (1H, s, HC=N); 4.68 (s, 2H, J = 1.8 Hz, C_5H_4), 4.67 (s, 2H C_5H_4). 4.07 (s, 5H, C_5H_5); 3.954 (3H, s, OCH_3); ^{13}C NMR ($CDCl_3$; δ ppm) 158.77 (HC=N); 85.18 (1C), 68.96 (4C) (Cp–C sub); 66.36 (Cp–C unsub); 69.62 (aliphatic C, –C_2H_4–); 56.09 (OCH_3).

2.2.3 Synthesis of 4,4′-((((ethane-1,2-diylbis(oxy))bis(2-ethoxy-1,4-phenylene))bis(methaneylylidene))bis(azaneylylidene))bisferrocene (Fcuc). The Schiff base **Fcuc** was synthesized by the aforementioned general procedure using (0.2 g, 0.740 mmol) of 4,4′-diformyl-bis-ethoxydiphenoxy ethane with (0.43 g, 1.5 mmol) 4-ferrocenyl aniline. Yield (67%); mp 201 °C; IR (ν cm^{-1}): ν(C=N) 1575; ν(C–O–C) 1226; ν(Fe–cp) 479. ^{1}H NMR ($CDCl_3$; δ ppm): 8.447 (1H, HC=N); 4.68 (s, 2H, J = 1.8 Hz, C_5H_4), 4.67 (s, 2H,J = 1.8, C_5H_4); 4.07 (s, 5H, C_5H_5); 3.954 (3H, s, OCH_3); 4.244 (2H, q,J = 6.9, $ArOCH_2$); 1.489 (3H, t,J = 6.9, CH_3); 4.338 (4H, s, –CH_2–) ^{13}C NMR ($CDCl_3$; δ ppm) 158.87 (HC=N); 85.18 (1C), 69.40, 68.96 (4C) (Cp–C sub); 66.36 (Cp–C unsub); 69.62 (aliphatic C, –C_2H_4–); 64.61 (OCH_2); 14.87 (CH_3).

2.3 Anticorrosion experiments

The chemical composition (wt%) of aluminium alloy (AA2219-T6) used for all experiments was as follows: Mn = 0.32; Cu = 6.48; Fe = 0.23; Ti = 0.06; Si = 0.49; V = 0.08; Zn = 0.04; Zr = 0.2 and balance of Al was used. Dimensions of sheets used for weight loss experiments as well as working electrode for electrochemical impedance spectroscopy (EIS) measurements were 1.2 × 1.1 × 0.46 cm^3. Proceeding to any test, the specimens of aluminium alloys were mechanically abraded with different grades emery paper. These sheets were degreased using acetone, washed with distilled water and then air dried before dipping in the cell of corrosive or/and anticorrosive medium. Analytical grade HCl of preset normality was used for the formation of a corrosive solution of 0.1 M HCl with triple distilled water. To ensure the solubility of all the biferrocenyl Schiff bases were dissolved in solution of 5% ethanol then from this specific concentration of solutions were prepared. The measurements were conducted in 40 mL of 0.1 M HCl in the absence and presence of 100 ppm Schiff bases.

2.4 Analysis

Glass vessel was used to carry out weight loss experiments having 30 mL of the anticorrosive and corrosive test solution for 6 hours at 25 °C. Aluminium alloy specimens of dimension 1.2 × 1.1 × 0.46 cm^3 were finely polished, dried and weighed. Then the substrates were dipped in 0.1 M HCl solution containing 100 ppm of inhibitor for 6 hours at 298 K. Aluminium alloy substrates were also submerged in 0.1 M of HCl without the addition of the anticorrosive compound. The surface of inhibited substrate was scratched to remove the adsorbed inhibitor, thoroughly washed with double distilled water, liquid soap followed by rinsing with triple distilled water and finally with acetone. After the washing process, the substrates were dried and weighed. The alloy substrate dipped in blank solution was also washed through the same procedure discussed previously but without scratching. Loss in weight of specimen was determined by finding the weight difference of the aluminium alloy substrates before and after insertion in the acidic medium.[33]

The corrosion rate (CR) was calculated (mg cm^{-2} h^{-1}) by the following eqn (1):

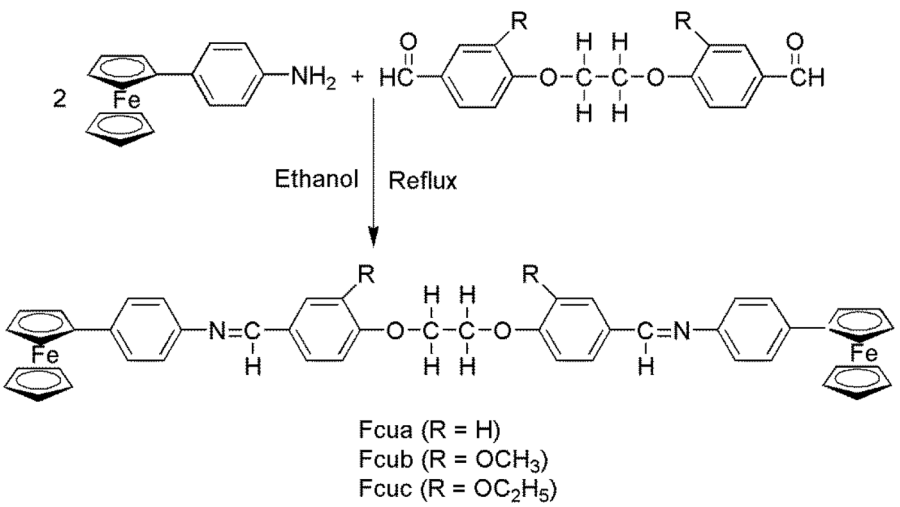

Scheme 1 Synthesis of ferrocenyl Schiff bases (**Fcua**, **Fcub**, **Fcuc**).

$$CR = \frac{\Delta W}{s \times t} \quad (1)$$

where, average weight loss is ΔW, t is the immersion time and s is the total area of the specimen. The inhibition efficiency (η) was obtained through the corrosion rate. The following eqn (2) is used to calculate percent inhibition efficiency (η%)

$$\eta\% = \left[\frac{CR^{\circ} - CR}{CR}\right] \times 100 \quad (2)$$

where, CR° and CR are the corrosion rates of the aluminium alloy substrate in the absence and presence of inhibitors, respectively and the degree of surface coverage (θ) was calculated through the following expression (3).

$$\theta = \frac{CR^{\circ} - CR}{CR^{\circ}} \quad (3)$$

A standard three electrode cell assembly was used for electrochemical measurements consisting of a pyrex glass flask with a flat bottom and three openings for reference, working and counter electrodes. Aluminium alloy (AA2219-T6) was used as a working electrode with 1.1 cm^2 of exposed surface area. Ag/AgCl and Pt wire were used as reference and counter electrode respectively. All experiments were conducted in an atmospheric condition without stirring. All the electrochemical measurements were conducted after 30 minutes of immersion time of aluminium alloy in the solution of electrolyte with and without the addition of anticorrosive material. The aluminium alloy substrate was dipped in the prepared solution until a stable value for open circuit potential (E_{ocp}) was obtained and measured. Gamry interface 1000 potentiostat/galvanostat system was used to conduct electrochemical measurements.

Electrochemical impedance spectroscopy (EIS) was used for impedance measurements by applying an AC signal of amplitude 10 mV in the frequency range from 100 kHz to 0.01 Hz. The investigation of the impedance spectra of Nyquist representation and fitting of the obtained results to equivalent circuits was performed. The diameter of the semicircle obtained in the Nyquist plot demonstrated the charge transfer resistance (R_{ct}). The inhibition efficiency percent η_{EIS} (%) was calculated from R_{ct} values with and without inhibitor addition using eqn (4).

$$\eta_{EIS}\ (\%) = \left[\frac{R_{ct} - R_{ct}^{\circ}}{R_{ct}}\right] \times 100 \quad (4)$$

where, charge transfer resistance R_{ct}° is without anticorrosive material and R_{ct} the charge transfer resistance value in the presence of anticorrosive material.

In the Tafel polarization measurement, polarization curves were obtained by changing the electrode potential from −0.67 to +0.67 mV with a scan rate of 1.0 mV s^{-1} at open circuit potential. Cathodic and anodic curves having linear Tafel segments were extrapolated that yielded an intersection point to get corrosion current density (i_{corr}) and corrosion potential (E_{corr}). In order to confirm the reproducibility of the results, each experiment was repeated thrice and the most reproducible results are accepted and reported. Inhibition efficiency percentage (η%) was calculated by using relevant i_{corr} values in place of rate of corrosion (CR) with the following eqn (5).[34]

$$\eta\% = \frac{i_{corr}^{\circ} - i_{corr}}{i_{corr}} \times 100 \quad (5)$$

2.5 Quantum chemical calculation

The geometrical optimization of the titled inhibitors was carried out using TURBOMOLE software,[35] while the quantum chemical calculations on the optimized structures were performed using Gaussian (09W) software package to gauge the efficiency of these compounds as corrosion inhibitors using a correlation between their molecular structure and inhibition efficiency. The theoretical parameters were calculated at the semi-empirical level using basis set PM6. The highest occupied molecular orbital energy (E_{HOMO}), the lowest unoccupied molecular orbital energy (E_{LUMO}), the energy gap ($\Delta E = E_{LUMO} - E_{HOMO}$), dipole moment ($\mu$), electronegativity, hardness and Mulliken charges of each inhibitor were also determined.

2.6 Surface analysis

FTIR-ATR was used for confirmation of the adsorption of biferrocene Schiff bases on surface of aluminium substrate using PerkinElmer System 2000. Vibrational frequency data of pure biferrocene Schiff bases and their adsorbed product on aluminium AA2219-T6 alloy after scratching it from the surface, was collected in the frequency range 4000–400 cm^{-1}.

The corroded surface morphology of the samples was observed by using a scanning electron microscope (SEM) TESCAN VEGA3 operating at 12 kV accelerating voltage. To investigate the surface morphology of the aluminium alloy AA2219-T6 in the absence and presence of anticorrosive materials, SEM images of polished aluminium alloy were taken before and after immersion in 0.1 M HCl in the absence and presence of 100 ppm of the inhibitor.

3 Results and discussion

The present biferrocenyl Schiff bases **Fcua**, **Fcub** and **Fcuc** were prepared according to synthetic route given in Scheme 1, by refluxing an ethanolic solution of biferrocenyl aniline with dialdehyde of different substitutions in (2.1 : 1) molar ratio, respectively. The products were obtained in 61–67% yield. All the synthesized biferrocenyl Schiff bases are soluble in many organic solvents such as ethanol, dimethylsulfoxide, dimethylformamide, chloroform and partially soluble in methanol.

3.1 Physical characterization

The FT-IR spectra of the biferrocenyl Schiff bases were recorded in 4000–400 cm^{-1} range. In all spectra of the biferrocenyl Schiff bases, the disappearance of aldehydic carbonyl C=O signal around 1680 cm^{-1} and appearance of the new azomethine C=N band at (1602, 1580 and 1575) cm^{-1} indicated the formation of Schiff base linkages for **Fcua**, **Fcub** and **Fcuc**, respectively. Moreover, the disappearance of peaks in the region 3390–3465

(asymmetric) and 3313–3369 (symmetric) cm^{-1} for $-NH_2$ moiety confirmed the conversion of amino group into azomethine bond. The stretching vibration of ether C–O–C linkage appeared around 1226–1240 cm^{-1} for all biferrocenyl Schiff bases. The stretching frequencies around 2860–2873 cm^{-1} corresponded to aliphatic C–H. Aromatic ring vibrations appeared at 1506–1509 cm^{-1} because of C=C. The stretching vibration corresponded to aromatic =C–H ranges between 3078–3092 in all compounds. Bands around 1106–1126 cm^{-1} and 1024–1059 cm^{-1} are characteristics of cyclopentadienyl rings. The absorption band for Cp–Fe–Cp bond of biferrocenyl moiety appeared at 479–486 cm^{-1} for all the investigated biferrocenyl Schiff bases (see Fig. S3, S6 and S9 in the ESI†).

The ^{1}H-NMR spectra of biferrocenyl Schiff bases were recorded at room temperature in $CDCl_3$ solvent using TMS as a reference. The azomethine linkage proton signal appeared at 8.49, 8.46 and 8.44 ppm for **Fcua**, **Fcub** and **Fcuc**, respectively. All the biferrocenyl Schiff bases exhibited signal for the unsubstituted cyclopentadienyl (η_5-C_5H_5) ring as a singlet of high intensity at δ value 4.07 ppm for the investigated compounds, due to the chemically equivalent environment. In the case of substituted (η_5-C_5H_4) ring, two types of signals are observed around 4.67 and 4.68 ppm ($J = 1.8$ Hz) for **Fcua**; 4.68 and 4.67 ppm ($J = 1.8$ Hz) for **Fcub**; and 4.68 and 4.67 ppm ($J = 1.8$ Hz) for **Fcuc**. This downfield shift of substituted Cp ring is ascribed to electron attracting nature of the attached substituents. A singlet of methoxy protons for methoxy (OCH_3) substituted benzene ring of **Fcub** appeared at 3.95 ppm, whereas a triplet and quartet around (1.49, $J = 6.9$) and 4.244, $J = 6.9$) ppm, respectively, were observed in the case of ethoxy substituted Schiff base (**Fcuc**). Aromatic ring protons showed their characteristic signals in the range of (7.05–7.92, m, $J = 8.1$) for **Fcua**, (7.07–7.66, m, $J = 8.4$) for **Fcub** and (7.103–7.65, m, $J = 8.4$) for **Fcuc**. All biferrocenyl Schiff bases displayed singlet for aliphatic protons (C_2H_4) around 4.34–4.35 ppm (see Fig. S1, S4 and S7 in the ESI†).

The ^{13}C-NMR spectra of all the biferrocenyl Schiff bases were recorded at room temperature using $CDCl_3$ as a solvent. In ^{13}C-NMR spectra of the compounds, the signal for azomethine –HC=N– carbon, the most deshielded one, appeared at 159.14 ppm, 158.77 ppm and 158.87 ppm for **Fcua**, **Fcub** and **Fcuc**, respectively. The signal of $-CH_2-$ carbon appeared at 69.62–69.40 ppm. Carbon atoms of the substituted cyclopentadienyl ring appeared in the range of 85.09–85.18 ppm and 68.96–68.40, while unsubstituted cyclopentadienyl ring in the range of 66.36–66.38 ppm. The methoxy (OCH_3) carbon gives a signal at 56.09 ppm (**Fcub**), and for ethoxy (OC_2H_5) group two carbon signals appeared at 64.61 (OCH_2) and 14.87 (CH_3) in (**Fcuc**). The aromatic carbon atoms displayed their signals around 112–151.38 ppm for all the Schiff bases. Aliphatic carbon atoms in $-C_2H_4-$ showed characteristic singlet between 69.62–69.63 ppm for all the Schiff bases (see Fig. S2, S5 and S8 in the ESI†).

3.2 Cyclic voltammetry

Cyclic voltammetric (CV) measurements were performed to investigate the redox behaviour of biferrocenyl Schiff bases. The redox potential for biferrocenyl Schiff bases changes within broader limits, which depends upon the electron withdrawing or electron donating nature of the substituent. Hence, due to change in the substituent nature, the redox properties can drastically be affected.[7] The redox-potential for the ferrocene–ferrocenium couple ranges between 0.3–0.4 V.

The initial electrochemical studies of the biferrocenyl Schiff bases were conducted by cyclic voltammetry in DMF (0.1 M tetrabutylammonium perchlorate (TBAP), Pt as a counter electrode, Ag/AgCl as a reference electrode and GC as a working electrode). The voltammograms showed a couple of distinct and stable redox peaks in the potential range 0.0–1.0 V. The biferrocenyl Schiff bases **Fcua**, **Fcub** and **Fcuc** showed anodic peaks at 0.716 V, 0.635 V and 0.590 V, respectively and cathodic peaks at 0.446 V, 0.372 V and 0.428 V, respectively (Fig. 1(a–c) and Table 1). These redox peaks can be attributed to Fe(II)/Fe(III), showing a quasi-reversible process.[36,37] The half wave potential for **Fcua**, **Fcub** and **Fcuc** located at $E_{1/2} = 0.531$ V, 0.542 V and 0.522 V and the peak potential difference were $\Delta E_p = 0.270$ V, 0.263 V and 0.162 V, respectively. The decrease in values of ΔE_p reveals that the electron donating ability increases *i.e.* oxidation process increases by the substitution of electron donating groups attached to aromatic ring. As a result the inhibition efficiency of the inhibitors increases. The peak current ratio $I_{pa}/I_{pc} = 12.257$, 1.535 and 1.328 for **Fcua**, **Fcub** and **Fcuc**, respectively. This data suggested a quasi-reversible single electron transfer process.[38] The cyclic voltammograms were recorded at different scan rates 50, 75, 100, 150, and 200 mVs^{-1} showed a slight discrepancy in peak potential most likely due to the retardation of electron transfer of the redox species. The higher oxidation potential E_{pa} values of the biferrocenyl Schiff bases as compared to the pure ferrocene (0.49 V) suggested a strong electronic interaction between the substituents and ferrocene moieties. Moreover, it was observed that the electron-donating groups (**Fcub** & **Fcuc**) facilitate the oxidation process by decreasing E_{pa}.

3.3 Corrosion inhibition study

3.3.1 Gravimetric analysis. The experimental data of weight loss Δw, percentage inhibition efficiency (η%), corrosion rate (CR) and surface coverage (θ) for AA2219-T6 in 0.1 M HCl in the absence and presence of different biferrocenyl Schiff bases of different substitutions for 6 hours of exposure time and at 298 K are shown in Table 2. Corrosion rate was calculated by using eqn (1) given in Section 2.4. The data clearly shows that the inhibition efficiency order for the tested compounds is **Fcuc** > **Fcub** > **Fcua**. This increase in efficiency of the biferrocenyl Schiff bases is due to the different substituents attached to the aromatic rings. The corrosion inhibition efficiency of an anti-corrosive material is based on its capability to be adsorbed on the metal substrate surface. The rate of corrosion was inhibited by all the three biferrocenyl Schiff bases by adsorbing at the aluminium substrate *via* the non-bonding electrons on the heteroatoms, such as oxygen atom (–O–, $-OCH_3$, $-OC_2H_5$), nitrogen atom (>C=N) and π electrons on the aromatic rings and the ferrocene moiety. The number of electron donating

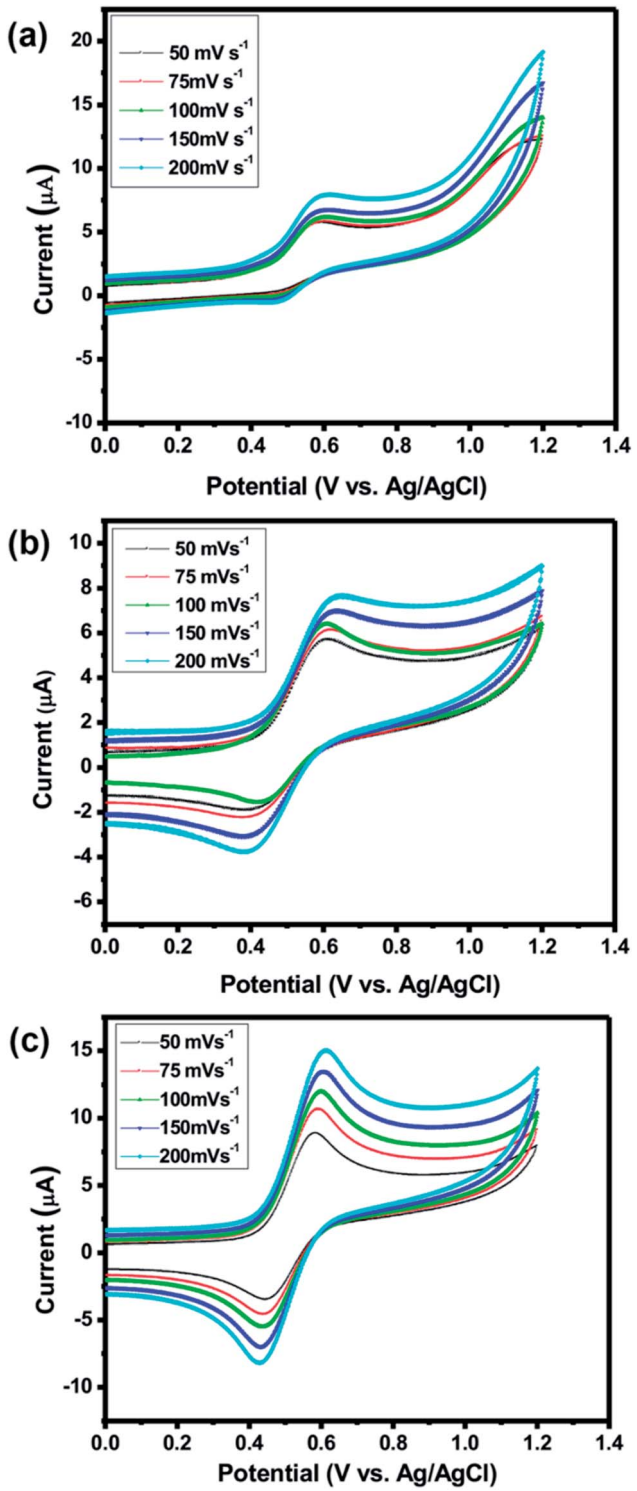

Fig. 1 Cyclic voltammogram of 10^{-3} M (a) **Fcua**, (b) **Fcub** and (c) **Fcuc** in 0.1 M TBAP at scan rates of 50, 75, 100, 150 and 200 mV s^{-1} using GC as a working electrode.

functional groups affects the adsorption affinity of the inhibitor, *i.e.*, with electron donating functional groups, the adsorption would be stronger, and inhibition efficiency would be higher. Thus, in the present case, **Fcub** showed higher protection ability than **Fcua** due to the presence of OCH_3 group and **Fcuc** revealed the maximum protection ability due to the presence of OC_2H_5 group. Therefore, the inhibition efficiency order was **Fcuc** > **Fcub** > **Fcua**. This is in accordance with the previously published reports on Schiff bases as corrosion inhibitors.[39,40]

Table 1 Electrochemical parameters of the biferrocenyl Schiff base compounds on glassy carbon electrode *vs.* Ag/AgCl in DMF at 200 mV s^{-1} scan rate at 25 °C temperature[a]

Compound	I_{pa} (μA)	I_{pc} (μA)	E_{pa} (V)	E_{pc} (V)	ΔE_p (V)	E° (V)	I_{pa}/I_{pc}
Fcua	5.381	0.439	0.716	0.446	0.270	0.531	12.257
Fcub	5.938	3.868	0.635	0.372	0.263	0.542	1.535
Fcuc	12.70	9.557	0.590	0.428	0.162	0.522	1.328

[a] I_{pa} = anodic peak current, I_{pc} = cathodic peak current, E_{pa} = anodic peak potential, E_{pc} = cathodic peak potential, E° = formal potential.

3.3.2 Electrochemical impedance measurements. The synthesized biferrocenyl Schiff bases (100 ppm) were employed for anticorrosion studies of the aluminum substrate AA2219-T6 (1 × 1 cm^2) in 0.1 M of HCl using electrochemical impedance spectroscopy (EIS) at open circuit potential. The impedance studies provided clear illustration of the corrosion inhibition kinetics of metallic substrates in terms of the Nyquist plot (Z_{real} *vs.* Z_{imag}).

Nyquist plots of all the inhibitors exhibited a semicircle shaped capacitive loop in high the frequency region and an inductive loop at the low frequency area as shown in Fig. 2(a). The semicircle indicated the formation of a barrier layer of the biferrocenyl Schiff bases on the alloy surface. Therefore, the charge transfer resistance associated with the corrosion activity and the behavior of the electrical double layer are elucidated. Stabilization of intermediates formed during the corrosion process may result in the formation of inductive loop,[41,42] however, the mechanism is still unclear. The deviation from the ideal semicircle is generally ascribed to the frequency scattering as well as non-homogeneity, roughness of the substrate surface, mass transport process and the resulting adsorption process.

Nyquist plots were comprehended further by fitting the experimental data to a simple equivalent circuit model as given in Fig. 2(b), which consists of the charge transfer resistance (R_{ct}), solution resistance (R_s), constant phase element (CPE), inductor and its corresponding resistance. CPE is used instead of ideal capacitor (for ideal cases, the CPE is equal to capacitor when n = 1) in order to account for the non-ideal behavior of the system.[43] Fig. 2(c) represents Nyquist plot of the blank (without inhibitor) having experimental fitted data for further comprehension of the simple equivalent circuit model. The Nyquist plots of aluminum alloy substrate in the absence and presence of substituted biferrocenyl Schiff bases are given in Fig. 2(a).

In case of EIS, the inhibition efficiency is calculated using charge transfer resistance values in eqn (4). As shown in Table 3, charge transfer resistance (R_{ct}) of the blank solution (0.1 M HCl) was estimated as 128.6 Ω cm^2 and for the biferrocenyl Schiff base inhibitors, it is 1630 Ω cm^2, 2390 Ω cm^2 and 3198 Ω cm^2, for **Fcua**, **Fcub** and **Fcuc**, respectively. The impedance

Table 2 Weight loss parameters for AA2219-T6 in 0.1 M HCl in the absence and presence of various Schiff bases

Codes	C_{inh} (ppm)	Δw (mg)	CR (mg cm^{-2} h^{-1})	η%	Degree of surface coverage (θ)
Blank	—	0.0051	1.5782	—	—
Fcua	100	0.0006	0.1893	88.00	0.8800
Fcub	100	0.0004	0.1262	92.00	0.9200
Fcuc	100	0.0001	0.0315	97.60	0.9760

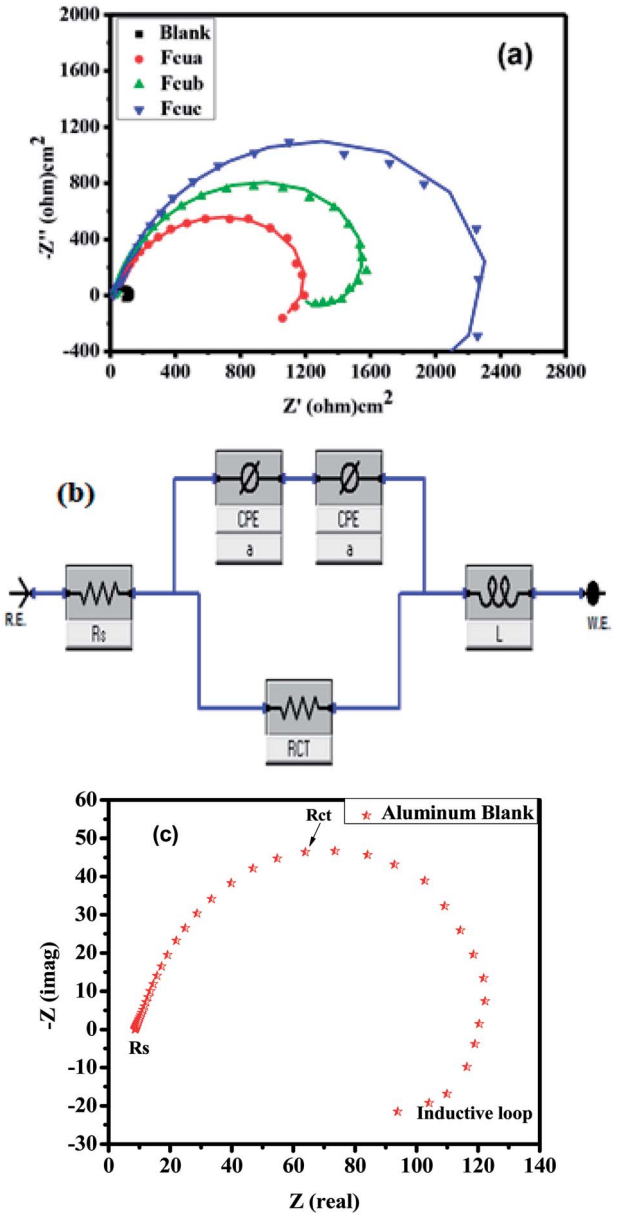

Fig. 2 (a) Overlay Nyquist plot of **Fcua**, **Fcub** and **Fcuc** recorded for aluminum in 0.1 M HCl, (b) electrical equivalent model used for simulation of the EIS data, and (c) Nyquist plot of the blank (without inhibitor).

parameters attained from the Nyquist plots and percentage of corrosion inhibition efficiencies are given in Table 3. The extent of corrosion of the aluminum alloy was perceived to decrease in the presence of biferrocenyl Schiff base inhibitor, which is depicted by the increased charge transfer resistance values for these anticorrosive compounds. The pronounced increase in R_{ct} values is imputed to the formation of an insulating protective film at the metal/solution interface. Hence, the higher R_{ct} values are affiliated with the slower corroding system.[44] The CPE of the blank solution (606.9×10^{-6} F cm^{-2}) is decreased to 239.4×10^{-6} F cm^{-2}, 52.85×10^{-6} F cm^{-2} and 163.7×10^{-6} F cm^{-2} for **Fcua**, **Fcub** and **Fcuc**, respectively. The decrease in CPE (C_{dl}) values can be assigned to a decrease in local dielectric constant and/or an increase in electrical double layer thickness, proposing that the biferrocenyl Schiff base inhibitor molecules are adsorbed at the metal/solution boundary.[45,46] A comparison of the capacitive loop of **Fcua**, **Fcub** and **Fcuc** indicates that ethoxy and methoxy substitutions have directly affected the anticorrosive efficiency of these biferrocenyl Schiff bases. The assessed inhibition efficiencies (η%) by using eqn (4) are 92%, 94% and 96% for **Fcua**, **Fcub** and **Fcuc**, respectively. These results confirm the superior corrosion inhibition property of **Fcuc** for aluminum corrosion in 0.1 M HCl due to the presence of electron donating ethoxy group (–OC_2H_5). The EIS results obtained are very much consistent with the weight loss measurement results. The following eqn (6) is used to calculate the double layer capacitance C_{dl} (μF cm^{-2});

$$C_{dl} = \frac{1}{2\pi f_m R_{ct}} \quad (6)$$

where, f_m (Hz) is the maximum frequency at the highest value of imaginary component of the Nyquist plot and R_{ct} is the charge transfer resistance in (Ω cm^2).

3.3.3 Tafel polarization measurements. The Tafel plots or potentiodynamic polarization measurements of AA2219-T6 alloy substrate were carried out in 0.1 M of HCl, in the absence and presence of the biferrocenyl Schiff bases at room temperature in order to study the anodic and cathodic reactions. Fig. 3 represents the polarization curves (Tafel plots) of AA2219-T6 alloy in 0.1 M HCl with and without anticorrosive

Table 3 Electrochemical parameters extracted from the equivalent circuit fits for aluminum alloy in the absence and presence of the biferrocenyl Schiff base inhibitors

Codes	R_{ct} (Ω cm^2)	C_{dl} (μF cm^{-2})	R_s (Ω cm^2)	η%
Blank	128.6	132.2	8.799	0.00
Fcua	1630.0	418.6	18.53	92.11
Fcub	2390.0	411.0	19.32	94.61
Fcuc	3198.0	217.2	25.27	95.97

biferrocenyl Schiff base compounds. The extracted electrochemical parameters *i.e.*, corrosion current density (i_{corr}), corrosion potential (E_{corr}), cathodic (b_c) and anodic (b_a) Tafel slopes associated with the polarization measurements of biferrocenyl Schiff bases are listed in Table 4. In order to determine polarization parameter, corrosion current density i_{corr} was extracted by extrapolating the linear section of the Tafel plots for anodic and cathodic lines to corrosion potential E_{corr}. Investigation of the data reveals no appreciable shift in the E_{corr} values in the presence of the anticorrosive biferrocenyl Schiff base compounds, which demonstrates that all the inhibitors acted as mixed type, that is some are anodic and others are cathodic in function. The observed variation in E_{corr} is much less than ±85 mV.[47] The value of corrosion current, i_{corr} obtained in pure 0.1 M HCl solution is found to be 18 500 μA cm^{-2}. By the addition of biferrocenyl Schiff base inhibitors, i_{corr} values are shifted towards lower side, indicating the anticorrosive effect of these inhibitors. As a result, the rate of corrosion decreases and inhibition efficiency of synthesized biferrocenyl Schiff base compounds increase.

Further, at a given applied potential the obvious decrease in the anodic and cathodic current densities indicates that these biferrocenyl Schiff base inhibitors inhibit both the hydrogen ions reduction as well as the anodic (metal) dissolution (Fig. 3). This proposes that all the examined biferrocenyl Schiff bases **Fcua**, **Fcub**, and **Fcuc** are mixed inhibitors and their inhibition efficiencies are 95.61%, 98.86% and 99.01%, respectively. Among all the examined Schiff bases, **Fcuc** shows the lowest corrosion current density i_{corr}, which renders it a good inhibitor having highest inhibition efficiency.[39,40] This is because of electron donating group ($-OC_2H_5$) attached to the aromatic ring. The order of increase in the inhibition efficiency of these biferrocenyl Schiff bases is **Fcuc** > **Fcub** > **Fcua**.

3.3.4 Quantum chemical calculations. To explore the effect of molecular structure on the inhibition behavior of the synthesized biferrocenyl Schiff bases, theoretical calculations were conducted using semi-empirical method in Gaussian 09 software package with PM6 basis set. The optimized molecular structures of the investigated biferrocenyl Schiff base corrosion inhibitors are given in Fig. 4. Additionally, frontier molecular orbital density distributions of the biferrocenyl Schiff base inhibitors (**Fcua**, **Fcub** and **Fcuc**) are depicted in Fig. 5. The molecular frontier orbitals play an important role in determining the electronic properties of the molecular systems. The chemical reactivity of these compounds depends upon the frontier molecular orbital (FMO), consisting of the highest occupied molecular orbital, HOMO, and the lowest unoccupied molecular orbital, LUMO.[48] A higher value of HOMO–LUMO energy gap indicates chemically stable molecules. Additionally, a larger HOMO–LUMO energy gap is shown by chemically hard molecules, indicating that the molecular systems resist changes in electronic configuration. The highest occupied molecular orbital energy (E_{HOMO}), the lowest unoccupied molecular orbital energy (E_{LUMO}), the energy gap ($\Delta E = E_{LUMO} - E_{HOMO}$), the dipole moment ($\mu$), electronegativity ($\chi$), softness ($\sigma$), hardness ($\eta$), and Mulliken charges were calculated in the semi-empirical calculations and are listed in Table S2.†

According to frontier molecular orbital theory, the electron donating ability of a molecule to appropriate electron acceptors is related to E_{HOMO}. Therefore, high values of E_{HOMO} point to an ease in adsorption and increase in inhibition efficiency (IE%). In the present case, a suitable acceptor with empty molecular orbitals (p orbital) is aluminum, to which the electrons are donated by biferrocenyl Schiff base inhibitors.[48,49] On the other hand, the value of E_{LUMO} is related to the electron accepting ability of the molecule. The lower values of E_{LUMO} indicate that these biferrocenyl Schiff base inhibitors can easily gain free electrons from the metal,[48] and thereby indicating a higher inhibition efficiency. From Table S2,† it can be seen that E_{HOMO} obeys the following order: **Fcuc** > **Fcub** > **Fcua**, which matches well with the inhibition efficiency. However, the order of E_{LUMO} does not agree with the inhibition efficiency, which may be attributed to the strong interaction between the investigated biferrocenyl Schiff bases and the aluminium alloy substrate.

Energy gap ($\Delta E = E_{LUMO} - E_{HOMO}$) is a very vital parameter that imparts activity of anticorrosive compound. Low values of ΔE provide high inhibition effectiveness, because less excitation energy is required to remove electrons from the last occupied orbital and the inhibitor also adsorbs more promptly.[50] According to Table S2,† **Fcub** has the lowest ΔE value as compared to **Fcua** and **Fcuc**. **Fcuc** also has the highest E_{HOMO} value as compared to **Fcua** and **Fcub**. Although all these biferrocenyl Schiff base compounds show comparable inhibition efficiencies, however, **Fcuc** and **Fcub** are more efficient inhibitors because of the presence of electron donating groups (ethoxy and methoxy). The HOMO of anticorrosive biferrocenyl Schiff bases appears mainly in the proximity of nitrogen and oxygen atoms. These atomic sites assist in the adsorption of the studied biferrocenyl Schiff bases on the aluminum alloy surface.

The HOMO and LUMO energies of the biferrocenyl Schiff bases are associated to the ionization potential (I) and electron affinity (A), respectively and are obtained from following equations.

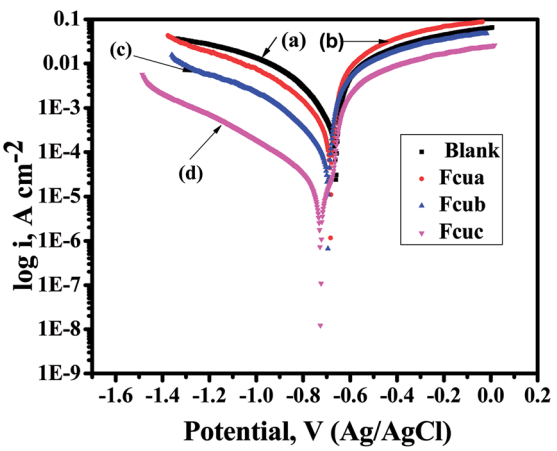

Fig. 3 Potentiodynamic polarization behaviour of the aluminium alloy in 0.1 M of HCl in the absence and presence of 100 ppm concentration of each biferrocenyl Schiff base corrosion inhibitor at 298 K.

Table 4 Polarization parameters for corrosion of aluminium alloy in 0.1 M of HCl in the presence and absence of the biferrocenyl Schiff bases at 298 K

Codes	E_{corr} (mV)	I_{corr} (μA cm^{-2})	β_a (V dec^{-1})	β_c (V dec^{-1})	Corrosion rate (CR) (mpy)	η%
Blank	−731.0	18 500	1.1970	1.793	8465	—
Fcua	−622.0	115.0	0.2427	0.409	52.66	95.61
Fcub	−624.1	29.50	0.2005	0.335	13.58	98.86
Fcuc	−726.0	23.00	0.2238	0.331	10.31	99.01

$$I = -E_{HOMO} \quad (7)$$

$$A = -E_{LUMO} \quad (8)$$

$$\eta = \frac{I - A}{2} \quad (9)$$

$$\chi = \frac{(I + A)}{2} \quad (10)$$

Eqn (9) and (10) were used to calculate the adiabatic global hardness (η) and adiabatic electronegativity (χ).

The chemical potential is indicated by the electronegativity (χ), and is related to the freedom of electrons in the inhibitors. A higher value of electronegativity (χ) reveals better inhibition performance. In this study, **Fcuc** shows the highest value of electronegativity χ, which is in good agreement with experimental results. The softness (σ) was computed through following eqn (11).

$$\sigma = \frac{1}{\eta} \quad (11)$$

According to hard and soft acid base (SHAB) concept,[51] a smaller value of global hardness (η) showed higher inhibition efficiency. Furthermore, dipole moment also plays an important role in corrosion inhibition. Greater the dipole moment of the inhibitor molecule, the higher is its corrosion efficiency.[52] **Fcub** and **Fcuc** have higher dipole moment than **Fcua**, as tabulated in Table S2.†

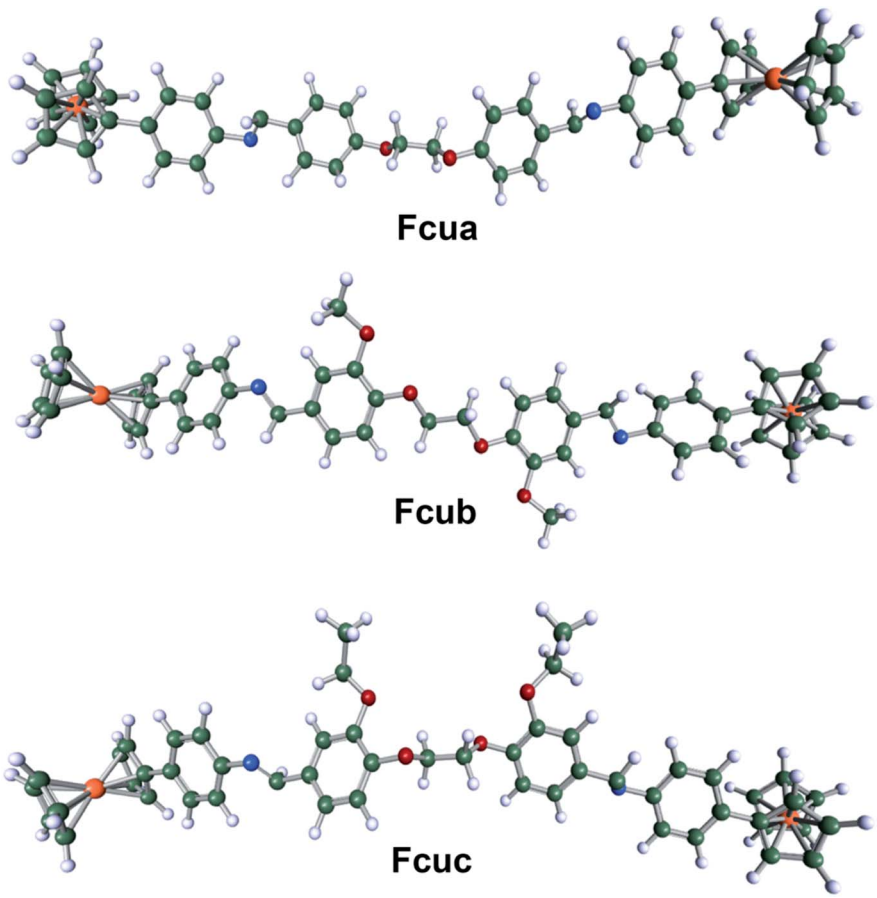

Fig. 4 Optimized structure of the biferrocenyl Schiff bases **Fcua**, **Fcub** and **Fcuc**.

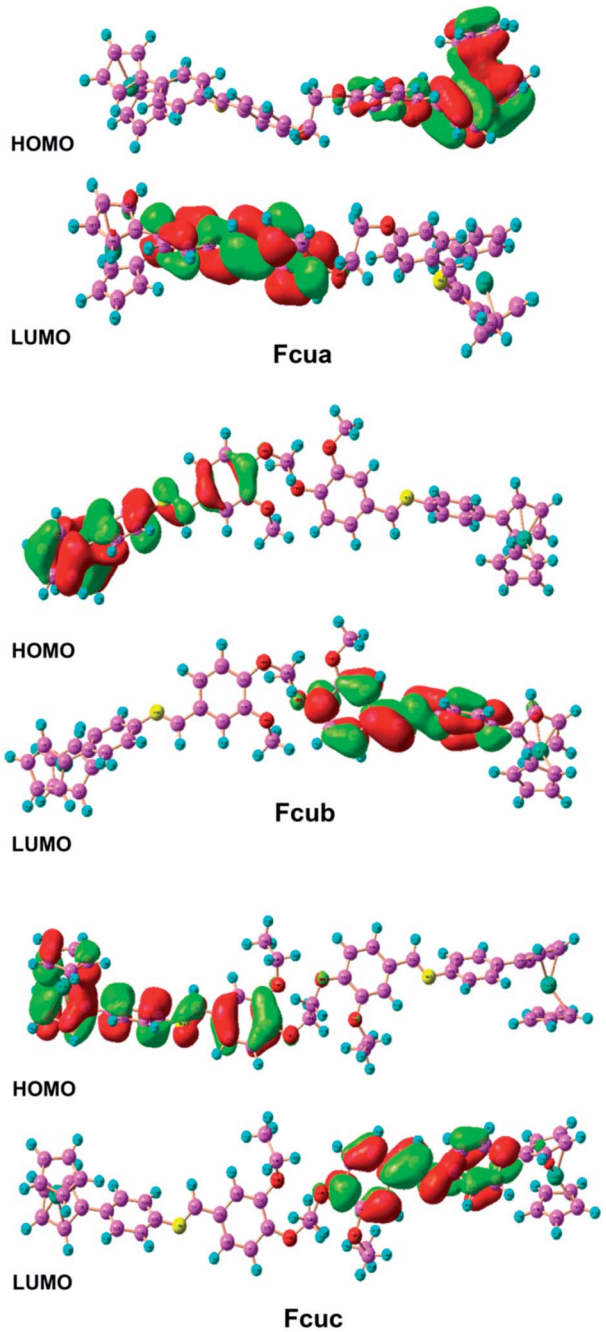

Fig. 5 Frontier molecular orbital density distribution of the biferrocenyl Schiff base inhibitors investigated in this work.

Mulliken charge population analysis gave the charge distribution over the ferrocenyl Schiff bases.[50] As shown in Fig. 6 and Table S2,† more negative charge densities are present on the oxygen and nitrogen atoms, which are responsible for a strong bond between the biferrocenyl Schiff bases and the metal substrate surface. In addition, adsorption occurs *via* the atoms having high negative charge densities. As evident from Table S2,† the presence of oxygen atom in the form of OC_2H_5 and OCH_3 groups in **Fcuc** and **Fcub**, respectively, caused a decrease in the electron density on N atom (qN83 and qN84) in imine (–C=N–) groups that are responsible for the chemisorption of these inhibitors. This result indicates that electrons are shared between N atoms and vacant p-orbitals of the aluminium. Therefore, the above-mentioned quantum chemical parameters obtained from a semi-empirical study of the biferrocenyl Schiff base inhibitors indicated similar results to our experimental inhibition efficiency tendency.

3.3.5 Surface analysis

3.3.5.1 FT-IR spectroscopy. FT-IR spectroscopy was performed in order to confirm the adsorption of the biferrocenyl Schiff bases as anticorrosive materials on aluminium AA2219-T6 alloy and the functional groups taking part in the adsorption mechanisms, the types of bond formed between the adsorbed anticorrosive material, their adsorption products on the aluminium alloy in acidic medium. For this purpose, the corrosion product with a biferrocenyl Schiff base inhibitor was scratched from the inhibited aluminium alloy surface. Fig. 7 shows the vibration frequency pattern of a representative anticorrosive material (**Fcua**) and its adsorption products on aluminium alloy surface. The stretching vibrations for the neat biferrocenyl Schiff base inhibitor are at 3092, 2870, 1602, 1569, 1376, 1449, 1240 and 486 cm^{-1}, that corresponds to Ar–CH stretch, $–CH_2–$, C=N, C–C stretches in ring, C–H rocking vibration, C–N stretch, C–O–C and Fe–Cp group, respectively. The stretching vibrations for the adsorbed biferrocenyl Schiff base were similar to that of neat anticorrosive material **Fcua** but with slight variation in the vibrational frequency pattern. The intensities of the absorption bands are decreased for the adsorbed biferrocenyl Schiff base compared with the neat biferrocenyl Schiff base. Some functional groups are shifted to the right or left, some are missing while some new functional groups are formed that strongly revealed the adsorption of biferrocene Schiff base inhibitor on aluminium alloy in 0.1 M HCl. The stretching vibrations for the adsorbed and free biferrocenyl Schiff base (**Fcua**) are tabulated in Table S1.† The stretching vibrations of the C=N and C–O–C are slightly shifted towards lower frequencies, indicating the interaction between unshared pair of electron on the nitrogen and oxygen atoms with the aluminium surface. Finally, we have observed that the cp rings peak intensities also became lowered upon adsorption on the aluminium surface.[53] A comparison of the FT-IR spectra of **Fcub** and **Fcuc** before and after adsorption on the aluminium alloy surface are shown in Fig. S10 and S11.†

3.3.5.2 SEM analysis. In the process of corrosion inhibition, the effect of inhibitors was investigated by SEM images of the aluminium AA2219-T6 alloy surface in the absence and presences of biferrocenyl Schiff bases. Fig. 8 shows the micrographs of the aluminium AA2219-T6 alloy surface. SEM images with clear lucid pictures of the polished alloy, corroded and inhibited with different magnification levels are shown in Fig. 8. The SEM micrograph of the fresh metal, *i.e.* the aluminium alloy surface before immersion appeared smooth and some abraded scratches, which are normally caused by emery paper, can be seen with magnification levels of (a1) 5 μm, (a2) 20 μm and (a3) 50 μm in Fig. 8. After immersion in the blank 0.1 M HCl solution for 6 h, the uniform aluminium alloy surface damaged severely and entirely covered with thick corrosion products and the

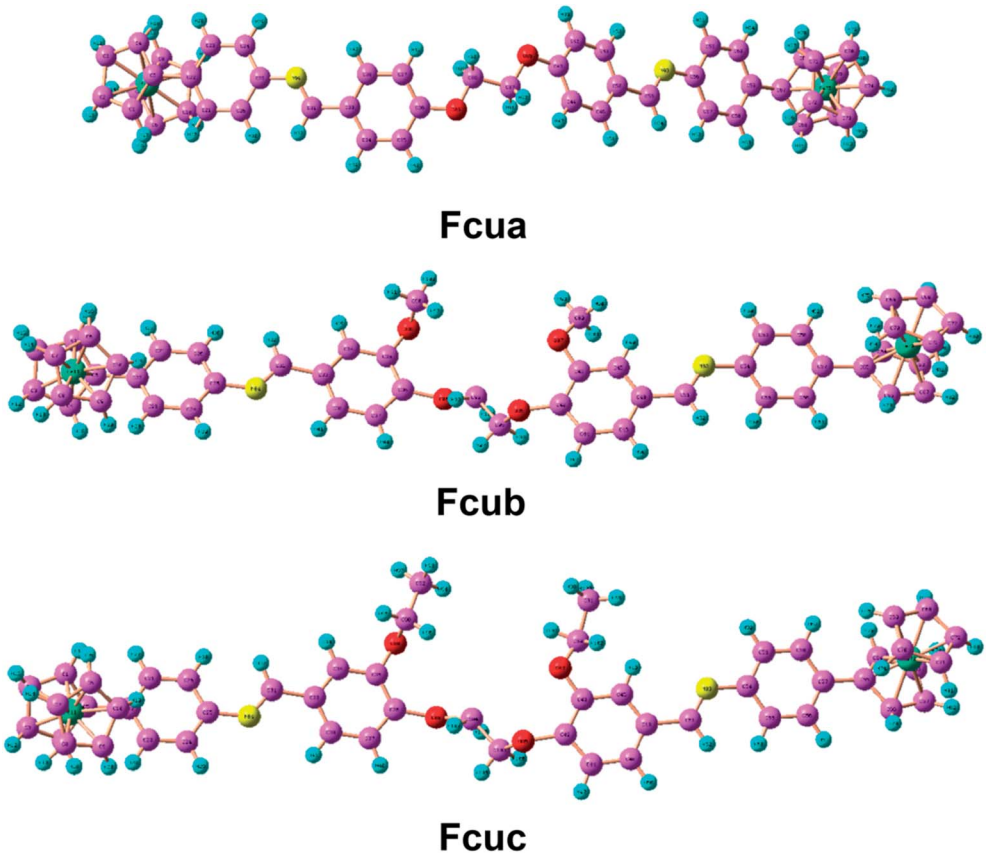

Fig. 6 Distribution of Mulliken charges in the biferrocenyl Schiff bases **Fcua**, **Fcub** and **Fcuc**.

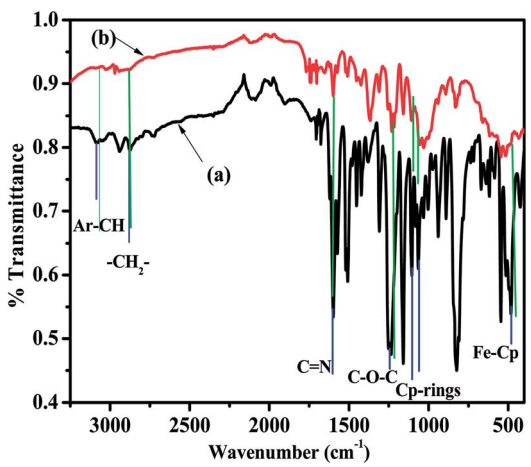

Fig. 7 (a) FT-IR spectra of neat **Fcua** (black) and (b) adsorbed **Fcua** (red) on the aluminium alloy surface in 0.1 M HCl solution.

surface of the metal substrate cannot be seen in (Fig. 8 (b1) 5 μm, (b2) 20 μm and (b3) 50 μm). The corroded layer of the specimen is rather uneven and very porous, in which there are some black holes. The aggressive ions can penetrate deep into the fresh aluminium surface through these black holes to form corrosion products after attacking it. After immersion in the biferrocenyl Schiff base inhibitor **Fcua** test solution for 6 h, an even surface was found for aluminium and a little damage occurred in (Fig. 8 (c1) 5 μm, (c2) 20 μm and (c3) 50 μm) as compared with the metal surface in the blank solution. Apparently, there is no corrosion product on the substrate surface, rather we found roughening scratches by emery paper proposing the efficient anticorrosive ability of the biferrocenyl Schiff base. Furthermore, comparing with the fresh metal surface in Fig. 8 (a1–a3), a good protective film is evident because of the biferrocenyl Schiff base adsorption on the surface of the metal substrate, which protects the destructive ions to attack its surface.

3.3.6 Mechanism of corrosion inhibition. The observation drawn from various procedures, one can infer that these biferrocenyl Schiff base anticorrosive materials are adsorbed on the surface of aluminium alloy to form a film that protect the substrate in medium of 0.1 M HCl. The inhibitive action can be explained on the basis of nitrogen and oxygen atoms besides π electron interaction of aromatic ring with the unshared p electrons of the aluminum metal. In azomethine, C=N the unshared pair of electron on nitrogen is easily available for sharing with metal atoms forming a covalent bond. Hence the biferrocenyl Schiff bases adsorbed and protect the surface of the metal from corrosion in acidic environment.

In the anticorrosion process, the adsorption of the biferrocenyl Schiff base anticorrosive material on the metallic substrate is the prime step in acidic medium. From the three

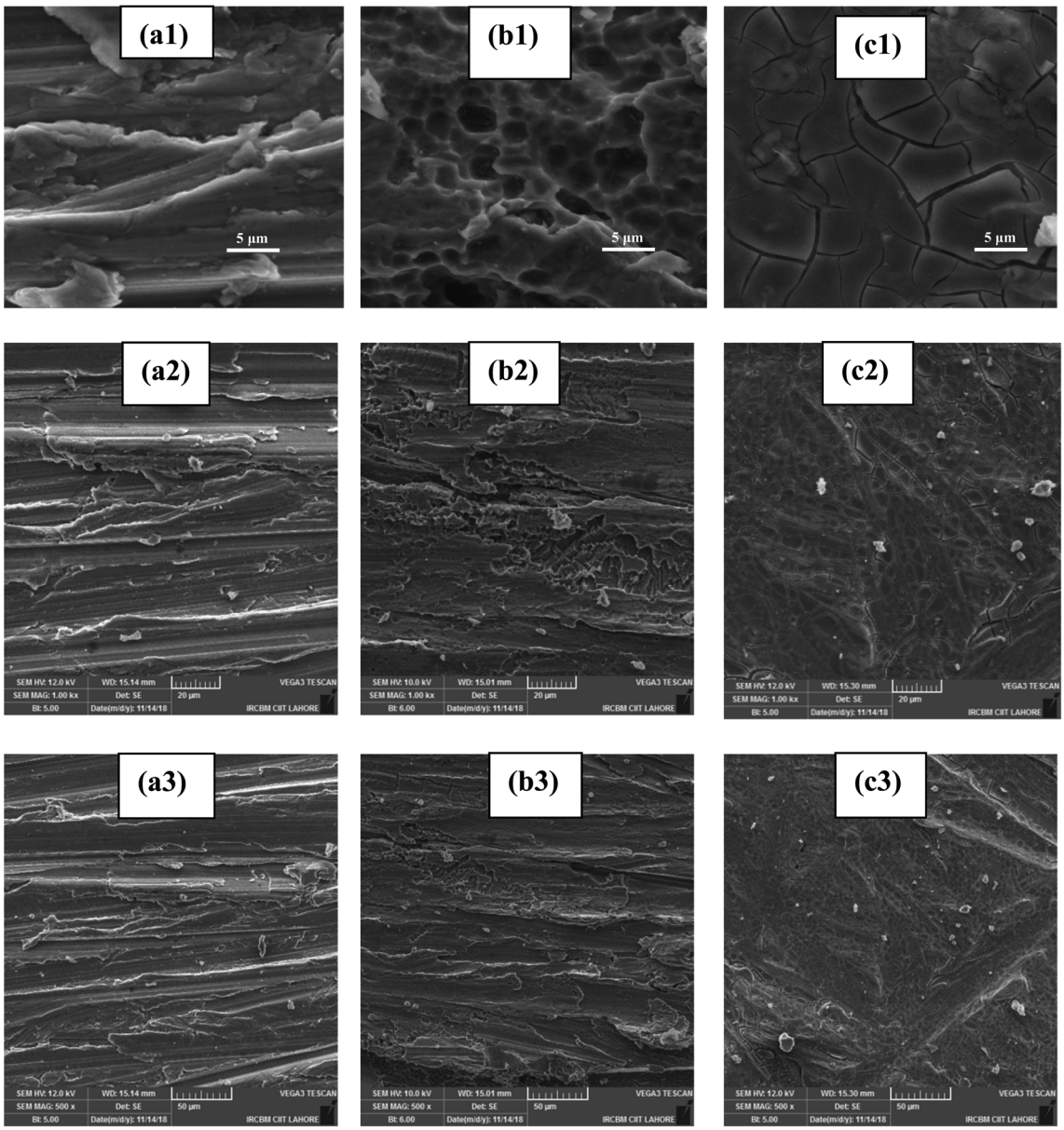

Fig. 8 SEM micrographs of the aluminium alloy surface (a1) 5 μm (a2) 20 μm and (a3) 50 μm polished AA2219-T6 alloy. (b1) 5 μm, (b2) 20 μm and (b3) 50 μm after immersion in 0.1 M HCl for 6 h (blank). (c1) 5 μm, (c2) 20 μm and (c3) 50 μm inhibited **Fcua** test solution.

types of interactions the process of adsorption may occur through one or more steps.[54,55] Three types of interactions are; electrostatic attraction between charged molecules and charged metal, coordination of metal atom with unshared paired of electrons of the adsorbing molecule, and π electrons participation of the anticorrosive molecule in the process of coordination. Generally, the examined ferrocene Schiff bases may be adsorbed on the aluminium substrate in their protonated or in neutral form. As aluminium surface is positively charged in 0.1 M HCl,[56,57] therefore it is assumed that Cl^- anion (of HCl) is first adsorbed on to the positively charged metal surface by coulombic attraction. Then afterwards, it is easier for protonated Schiff base to attack on the negatively charged surface of aluminium through electrostatic interaction between negatively charged aluminium surface and positively charged molecules. Adsorption on the aluminium alloy surface involves the displacement of aqueous molecules and sharing of electrons between the heteroatoms and aluminium alloy. Also, the anticorrosive molecules can adsorb on the surface of aluminium alloy on the basis of donor acceptor interactions between π-electrons of benzene rings and vacant p-orbitals of atoms of the aluminium surface.[33] These interactions assist in the formation of chemical bonds (also known as chemical adsorption or chemisorption). In acidic solution, protonation of Fe of the ferrocene molecule takes place and gain positive charge, which causes electrostatic attraction for the ferrocene Schiff base inhibitor on the negatively charged Aluminium metal substrate.[4] Thus, it is concluded that electrostatic interactions

as well as chemical adsorption are the main reason of aluminium alloy corrosion inhibition. Among all the investigated biferrocenyl Schiff bases in the present work, the presence of extra oxygen atoms and the chelate effect of **Fcub** and **Fcuc** is greater than **Fcua**. This is due to the presence of two electron donating groups of ($-OCH_3$) and ($-OC_2H_5$) in **Fcub** and **Fcuc**, respectively.[33] A comparative data of the inhibition efficiency of these biferrocenyl Schiff bases with previously published various ferrocene derivatives on different metal substrates and in different acidic conditions, are presented in Table S3 in the ESI.†

4 Conclusions

In quest of unexplored organometallic corrosion inhibitors, three biferrocenyl Schiff bases were synthesized, which contain large number of heteroatoms, aromatic rings, cover high surface area and organometallic moieties. Their structure was interpreted on the basis of FT-IR, ^1H and ^{13}C NMR spectroscopy. These synthesized organometallic biferrocenyl Schiff bases were symbolized as good anticorrosive materials for aluminium AA2219-T6 alloy in 0.1 M HCl solution. In the present investigation, the outcome obtained from experimental studies (electrochemical as well as gravimetric analysis) clearly manifested that the effects exerted by the heteroatoms, azomethine linkage and π-electrons provide most dominating role in the adsorption of the inhibitor molecules on the aluminium alloy surface. The weight loss measurements showed that all compounds efficiently inhibited the aluminium alloy corrosion. Polarization studies showed that all these biferrocenyl Schiff bases as mixed type inhibitors, having dominant cathodic action. Anticorrosive efficiency acquired using weight loss, polarization and EIS studies were in good agreement and in accordance with the order: **Fcuc** > **Fcub** > **Fcua** for AA2219-T6 alloy. This was because of the number of additional electron donating functional groups OCH_3 and OC_2H_5 attached to **Fcub** and **Fcuc**, resulting in higher inhibition efficiency. Quantum chemical calculations was used to determine E_{HOMO}, E_{LUMO}, dipole moment and Mulliken charge, confirming a strong bond between inhibitors and metal surface. Images of SEM showed an even surface for inhibited alloy sample than corrosive sample due to the development of shielding barrier film. FT-IR spectroscopy confirmed chemisorption of these biferrocenyl Schiff bases on the surface of aluminium alloy. The anticorrosive materials with diverse substitutions that play vital role in anticorrosion have been reported in this article for the first time for aluminium AA2219-T6 alloy.

Conflicts of interest

There are no conflicts to declare.

Acknowledgements

U. N. is highly obliged to the Higher Education Commission (HEC) of Pakistan (Pin No. 112-25825-2Ps1-592) for providing scholarship under the program 5000 Indigenous PhD Scholarships and to the Department of Chemistry Quaid-i-Azam University Islamabad, Pakistan for providing research facilities. F. U. S. is grateful for the financial support of the Norrbotten Research Council (NoFo 19-100).

References

1 Y. T. Liu, G. D. Lian, D. W. Yin and B. J. Su, Synthesis, characterization and biological activity of ferrocene-based Schiff base ligands and their metal(II) complexes, *Spectrochim. Acta, Part A*, 2013, **100**, 131–137.
2 M. Shabbir, Z. Akhter, I. Ahmad, S. Ahmed, M. Bolte, H. Ismail and B. Mirza, Ferrocene-based Schiff bases copper(II) complexes: synthesis, characterization, biological and electrochemical analysis, *Inorg. Chim. Acta*, 2017, **463**, 102–111.
3 Y.-T. Liu, G.-D. Lian, D.-W. Yin and B.-J. Su, Synthesis, characterization and biological activity of ferrocene-based Schiff base ligands and their metal(II) complexes, *Spectrochim. Acta, Part A*, 2013, **100**, 131–137.
4 M. S. Morad and A. A. O. Sarhan, Application of some ferrocene derivatives in the field of corrosion inhibition, *Corros. Sci.*, 2008, **50**, 744–753.
5 T. Höcher, A. Cinquantini, P. Zanello and E. Hey-Hawkins, Novel [3]ferrocenophanes: syntheses, redox properties and molecular structures of $[Fe\{(\eta^5\text{-}C_5H_4)CMe_2\}_2PR]$ (R = Ph, Cy), *Polyhedron*, 2005, **24**, 1340–1346.
6 C. Ornelas, Application of ferrocene and its derivatives in cancer research, *New J. Chem.*, 2011, **35**, 1973–1985.
7 S. R. Gupta, P. Mourya, M. M. Singh and V. P. Singh, Synthesis, structural, electrochemical and corrosion inhibition properties of two new ferrocene Schiff bases derived from hydrazides, *J. Organomet. Chem.*, 2014, **767**, 136–143.
8 H. Ünver and Z. Hayvali, Synthesis, spectroscopic studies and structures of square-planar nickel(II) and copper(II) complexes derived from 2-{(Z)-[furan-2-ylmethyl]imino] methyl}-6-methoxyphenol, *Spectrochim. Acta, Part A*, 2010, **75**, 782–788.
9 S. Fery-Forgues and B. Delavaux-Nicot, Ferrocene and ferrocenyl derivatives in luminescent systems, *J. Photochem. Photobiol., A*, 2000, **132**, 137–159.
10 Y. Zhou, S. Xu, L. Guo, S. Zhang, H. Lu, Y. Gong and F. Gao, Evaluating two new Schiff bases synthesized on the inhibition of corrosion of copper in NaCl solutions, *RSC Adv.*, 2015, **5**, 14804–14813.
11 Q. Deng, H.-W. Shi, N.-N. Ding, B.-Q. Chen, X.-P. He, G. Liu, Y. Tang, Y.-T. Long and G. R. Chen, Novel triazolyl bis-amino acid derivatives readily synthesized via click chemistry as potential corrosion inhibitors for mild steel in HCl, *Corros. Sci.*, 2012, **57**, 220–227.
12 Y. Yan, W. Li, L. Cai and B. Hou, Electrochemical and quantum chemical study of purines as corrosion inhibitors for mild steel in 1 M HCl solution, *Electrochim. Acta*, 2008, **53**, 5953–5960.

13 S. Safak, B. Duran, A. Yurt and G. Turkoglu, Schiff bases as corrosion inhibitor for aluminium in HCl solution, *Corros. Sci.*, 2012, **54**, 251–259.
14 M. Lashgari, M.-R. Arshadi and S. Miandari, The enhancing power of iodide on corrosion prevention of mild steel in the presence of a synthetic-soluble Schiff-base: electrochemical and surface analyses, *Electrochim. Acta*, 2010, **55**, 6058–6063.
15 S. Shahabi, P. Norouzi and M. R. Ganjali, Theoretical and Electrochemical Study of Carbon Steel Corrosion Inhibition in the Presence of Two Synthesized Schiff Base Inhibitors: Application of Fast Fourier Transform Continuous Cyclic Voltammetry to Study the Adsorption Behavior, *Int. J. Electrochem. Sci.*, 2015, **10**, 2646–2662.
16 P. Deepa and R. Padmalatha, Corrosion behaviour of 6063 aluminium alloy in acidic and in alkaline media, *Arabian J. Chem.*, 2017, **10**, S2234–S2244.
17 N. S. Ayati, S. Khandandel, M. Momeni, M. H. Moayed, A. Davoodi and M. Rahimizadeh, Inhibitive effect of synthesized 2-(3-pyridyl)-3,4-dihydro-4-quinazolinone as a corrosion inhibitor for mild steel in hydrochloric acid, *Mater. Chem. Phys.*, 2011, **126**, 873–879.
18 J. Aljourani, K. Raeissi and M. A. Golozar, Benzimidazole and its derivatives as corrosion inhibitors for mild steel in 1 M HCl solution, *Corros. Sci.*, 2009, **51**, 1836–1843.
19 H. M. Abd El-Lateef, Experimental and computational investigation on the corrosion inhibition characteristics of mild steel by some novel synthesized imines in hydrochloric acid solutions, *Corros. Sci.*, 2015, **92**, 104–117.
20 P. Shetty, Hydrazide Derivatives: An Overview of Their Inhibition Activity against Acid Corrosion of Mild Steel, *S. Afr. J. Chem.*, 2018, **71**, 46–50.
21 A. K. Singh and M. A. Quraishi, Effect of Cefazolin on the corrosion of mild steel in HCl solution, *Corros. Sci.*, 2010, **52**, 152–160.
22 F. B. Ravari, A. Dadgarinezhad and I. Shekhshoaei, Investigation on two salen type schiff base compounds as corrosion inhibition of copper in 0.5 M H_2SO_4, *Gazi University Journal of Science*, 2009, **22**, 175–182.
23 S. P. Fakrudeen, Electrochemical investigation of corrosion inhibition of AA6063 alloy in 1 M hydrochloric acid using Schiff base compounds, *IOSR J. Appl. Chem.*, 2012, **2**, 37–47.
24 N. Belhadj, A. Ourari, S. Keraghel, B. Schöllhorn and D. Matt, Crystal Structure and Corrosion Inhibition Properties of Ferrocenyl- and Phenylendiamine-Iminomethylphenoxy Cobalt Complexes, *J. Chem. Crystallogr.*, 2017, **47**, 40–46.
25 H. Heydari, M. Talebian, Z. Salarvand, K. Raeissi, M. Bagheri and M. A. Golozar, Comparison of two Schiff bases containing O-methyl and nitro substitutes for corrosion inhibiting of mild steel in 1 M HCl solution, *J. Mol. Liq.*, 2018, **254**, 177–187.
26 S. Bonetti, R. Spengler, A. Petersen, L. S. Aleixo, A. A. Merlo and S. M. Tamborim, Surface-decorated silica with Schiff base as an anticorrosive coating for aluminium alloy 2024-T3, *Appl. Surf. Sci.*, 2019, **475**, 684–694.
27 S. Fatima, R. Sharma, F. Asghar, A. Kamal, A. Badshah and H.-B. Kraatz, Study of New Amphiphiles based on Ferrocene containing Thioureas as Efficient Corrosion Inhibitors: Gravimetric, Electrochemical, SEM and DFT Studies, *J. Ind. Eng. Chem.*, 2019, **76**, 374–387.
28 T. Zaiz and T. Lanez, Corrosion inhibition of carbon steel XC70 in H_2SO_4 solution by ferrocene derivative 3-(ferrocenylmethylamine)benzonitrile, *J. Fundam. Appl. Sci.*, 2015, **4**, 182.
29 U. Nazir, Z. Akhter, N. Z. Ali and F. U. Shah, Experimental and theoretical insights into the corrosion inhibition activity of novel Schiff bases for aluminum alloy in acidic medium, *RSC Adv.*, 2019, **9**, 36455–36470.
30 A. Aytaç, Ü. Özmen and M. Kabasakaloğlu, Investigation of some Schiff bases as acidic corrosion of alloy AA3102, *Mater. Chem. Phys.*, 2005, **89**, 176–181.
31 G. Greber, Vogel's textbook of practical organic chemistry (5th ed.), revised by Brian S. Furniss, Antony J. Hannaford, Peter W. G. Smith and Austin R. Tatchell, John Wiley & Sons, New York, 1514 pp., *J. Polym. Sci., Part A: Polym. Chem.*, 1991, **29**, 1223.
32 P. Hu, K.-Q. Zhao and H.-B. Xu, 4-Nitrophenylferrocene, *Molecules*, 2001, **6**, M249.
33 S. P. Fakrudeen, A. Murthyh. C, B. Raju V, H. C. Ananda Murthy and V. Bheema Raju, Corrosion inhibition of AA6061 and AA6063 alloy in hydrochloric acid media by Schiff base compounds, *J. Chil. Chem. Soc.*, 2012, **57**, 1364–1371.
34 M. Behpour, S. M. Ghoreishi, N. Soltani and M. Salavati-Niasari, The inhibitive effect of some bis-N,S-bidentate Schiff bases on corrosion behaviour of 304 stainless steel in hydrochloric acid solution, *Corros. Sci.*, 2009, **51**, 1073–1082.
35 *TURBOMOLE V7.0 2015, a development of University of Karlsruhe and Forschungszentrum Karlsruhe GmbH, 1989-2007*, TURBOMOLE GmbH, since 2007.
36 M. Lamač, I. Císařová and P. Štěpnička, Preparation, coordination and catalytic use of planar-chiral monocarboxylated dppf analogues, *New J. Chem.*, 2009, **33**, 1549–1562.
37 I. Damljanović, M. Čolović, M. Vukićević, D. Manojlović, N. Radulović, K. Wurst, G. Laus, Z. Ratković, M. Joksović and R. D. Vukićević, Synthesis, spectral characterization and electrochemical properties of 1*H*-3-(*o*-, *m*- and *p*-ferrocenylphenyl)-1-phenylpyrazole-4-carboxaldehydes, *J. Organomet. Chem.*, 2009, **694**, 1575–1580.
38 P. T. Kissinger and W. R. Heineman, Cyclic voltammetry, *J. Chem. Educ.*, 1983, **60**, 702.
39 A. Singh, K. R. Ansari, J. Haque, P. Dohare, H. Lgaz, R. Salghi and M. A. Quraishi, Effect of electron donating functional groups on corrosion inhibition of mild steel in hydrochloric acid: experimental and quantum chemical study, *J. Taiwan Inst. Chem. Eng.*, 2018, **82**, 233–251.
40 A. Aytaç, Cu(II), Co(II) and Ni(II) complexes of –Br and ethoxy substituted Schiff bases as corrosion inhibitors for aluminium in acidic media, *J. Mater. Sci.*, 2010, **45**, 6812–6818.
41 A. Khadraoui, A. Khelifa, L. Touafri, H. Hamitouche and R. Mehdaoui, Acid extract of Mentha pulegium as

a potential inhibitor for corrosion of 2024 aluminum alloy in 1 M HCl solution, *J. Mater. Environ. Sci.*, 2013, **4**, 663–670.
42 S. S. Abd El Rehim, H. H. Hassan and M. A. Amin, Corrosion inhibition of aluminum by 1,1(lauryl amido)propyl ammonium chloride in HCl solution, *Mater. Chem. Phys.*, 2001, **70**, 64–72.
43 J. R. Macdonald, Impedance spectroscopy, *Ann. Biomed. Eng.*, 1992, **20**, 289–305.
44 H. Ashassi-Sorkhabi, D. Seifzadeh and M. G. Hosseini, EN, EIS and polarization studies to evaluate the inhibition effect of 3H-phenothiazin-3-one, 7-dimethylamin on mild steel corrosion in 1 M HCl solution, *Corros. Sci.*, 2008, **50**, 3363–3370.
45 S. K. Singh, S. P. Tambe, G. Gunasekaran, V. S. Raja and D. Kumar, Electrochemical impedance study of thermally sprayable polyethylene coatings, *Corros. Sci.*, 2009, **51**, 595–601.
46 X. Li and S. Deng, Inhibition effect of Dendrocalamus brandisii leaves extract on aluminum in HCl, phosphoric acid solutions, *Corros. Sci.*, 2012, **65**, 299–308.
47 S. Banerjee, A. Mishra, M. M. Singh, B. Maiti, B. Ray and P. Maiti, Highly efficient polyurethane ionomer corrosion inhibitor: The effect of chain structure, *RSC Adv.*, 2011, **1**, 199–210.
48 R. Padash, M. R. Nasrabadi, A. Shokuhi, R. Ali, S. Nasab and T. Jesionowski, A theoretical study of two novel Schiff bases as inhibitors of carbon steel corrosion in acidic medium, *Appl. Phys. A*, 2019, **125**, 78.
49 K. F. Khaled, Monte Carlo simulations of corrosion inhibition of mild steel in 0.5 M sulphuric acid by some green corrosion inhibitors, *J. Solid State Electrochem.*, 2009, **13**, 1743–1756.
50 I. B. Obot and Z. M. Gasem, Theoretical evaluation of corrosion inhibition performance of some pyrazine derivatives, *Corros. Sci.*, 2014, **83**, 359–366.
51 L. Herrag, B. Hammouti, S. Elkadiri, A. Aouniti, C. Jama, H. Vezin and F. Bentiss, Adsorption properties and inhibition of mild steel corrosion in hydrochloric solution by some newly synthesized diamine derivatives: experimental and theoretical investigations, *Corros. Sci.*, 2010, **52**, 3042–3051.
52 A. Popova, M. Christov, S. Raicheva and E. Sokolova, Adsorption and inhibitive properties of benzimidazole derivatives in acid mild steel corrosion, *Corros. Sci.*, 2004, **46**, 1333–1350.
53 N. Nnaji, N. Nwaji and J. Mack, Corrosion Resistance of Aluminum against Acid Activation: Impact of Benzothiazole-Substituted Gallium Phthalocyanine, *Molecules*, 2019, **24**, 1–22.
54 V. R. Saliyan and A. V. Adhikari, Quinolin-5-ylmethylene-3-{[8-(trifluoromethyl)quinolin-4-yl]thio}propanohydrazide as an effective inhibitor of mild steel corrosion in HCl solution, *Corros. Sci.*, 2008, **50**, 55–61.
55 D. Paul Schweinsberg, G. A. George, A. K. Nanayakkara and D. A. Steinert, The protective action of epoxy resins and curing agents—inhibitive effects on the aqueous acid corrosion of iron and steel, *Corros. Sci.*, 1988, **28**, 33–42.
56 A. Yurt, S. Ulutas and H. Dal, Electrochemical and theoretical investigation on the corrosion of aluminium in acidic solution containing some Schiff bases, *Appl. Surf. Sci.*, 2006, **253**, 919–925.
57 A. K. Vijh, Chemical Approaches to the Approximate Prediction of Band Gaps of Binary Semiconductors and Insulators, *J. Electrochem. Soc.*, 2007, **117**, 173C.